Chapter 3

An antiparallel tetrameric coiled coil

Zheng, T. T.; Bulacu, M.; Boyle, A.; Versluis, F.; Marsden, H. R.; Valdink, D.; Martelli, G.; Raap, J.; Sevink, A.; Kros, A., An antiparallel tetrameric coiled coil. Manuscript in preparation.

Abstract

The complementary peptides Coil-K and Coil-E were designed to assemble into a heterodimeric coiled coil. In this chapter the effect of reversing the amino acid sequence of peptide Coil-E on complex formation with peptide Coil-K was investigated. Coiled coil assembly was studied using multiple techniques including circular dichroism, paramagnetic proton NMR, steady state fluorescence spectroscopy measurements, sedimentation equilibrium analytical ultracentrifugation and computational simulations. All results show that the reversed peptide Coil-E_r folds with Coil-K to form a stable antiparallel coiled coil tetramer and not an antiparallel heterodimer as previously reported. Thus, this study shows that reversing the amino acid sequence of coiled coil peptides can strongly affect the self-assembly process. Cholesterol modified peptide Coil-K and Coil-E_r were tested as a model system for membrane fusion and its fusogenity was compared to the original model system. Lipid and content mixing assays showed no significant difference between the heterodimeric and the tetramer coiled coil mediated fusion. This indicates that peptide orientation and oligomerization state does not influence this model system for membrane fusion.

Introduction

One of the most important vital vesicle trafficking processes is SNARE-dependent (SNARE: soluble N-ethylmaleimide-sensitive factor attachment protein receptor) membrane fusion.[1-3] There are three key steps in this process: membrane surface conjugated SNARE proteins self-assemble as SNAREpins (a four-helix SNARE proteins coiled coil bundle), followed by docking of the two opposing lipid membrane resulting in full fusion and content transfer.[4]

One of the reduced SNARE membrane fusion models is based on the complementary peptide pair Coil-K ($[KIAALKE]_3$) and Coil-E ($[EIAALEK]_3$).[5] These two peptides were designed to assemble into a parallel heterodimeric coiled coil. In this reduced peptide-induced membrane fusion model, the SNARE proteins are mimicked by lipidated conjugates of Coil-K and Coil-E.[6-9] Upon mixing equimolar amounts of Coil-E modified liposomes with Coil-K liposomes, parallel coiled coil formation (CC-K/E) forces the two opposing membrane into close proximity resulting in full fusion of the liposomes.[10, 11]

Recently, there were two contradictory studies with the point of contention that whether the parallel zipper-like coiled coil motif orientation is required for membrane fusion. Two different approaches were used to design a non-zipper-like coiled coil motif orientation: the Diederichsen group designed an anti-parallel coiled coil motif in which the membrane anchor is located at both peptides C-terminus; while Kros designed parallel coiled coil forming peptides in which the membrane anchor is located at opposite peptide termini (See Appendix Figure A1).[12, 13] In the first approach it was shown that a non-zipper-like coiled coil assembly inhibits membrane fusion, indicating the necessity of a zipper-like coiled coil orientation in the fusion process similar to the SNARE protein mediated fusion; In contrast, Kros showed that a non-zipper-like coiled coil motif also induces membrane fusion, indicating that the coiled coil orientation (i.e. parallel vs antiparallel) does not affect the rate of fusion with these short peptides. It is important to note that while the Kros group used the original Coil-K/Coil-E (CC-K/E) peptides; the Diederichsen group used Coil-E with a reversed amino acid sequence (i.e. Coil-E_r). It was hypothesized that Coil-K with Coil-E_r ($[KELAAIE]_3$) would form an antiparallel dimeric coiled coil. However no experimental data supporting this assumption was given.

The effect of reversing the amino acid primary sequence on self-assembly behavior has been studied before.[14-16] However most of these studies on inverted protein/peptide focused on single protein/peptide intramolecular interactions and not on heterodimeric coiled coil motifs.[17] Therefore we set out to study the assembly of Coil-K and Coil-E_r and to find out whether an antiparallel heterodimer is formed (Scheme 1).

For this, a variety of spectroscopic techniques were used to study the coiled coil assembly of Coil-E and Coil-E_r with Coil-K. Circular Dichroism (CD) showed that the peptides Coil-E and Coil-E_r have a similar α-helical secondary structure. However, when mixed with an equimolar amount of Coil-K, different coiled coil assemblies were observed. While Coil-K and Coil-E form a parallel dimer, Coil-K and Coil-E_r assemble into an antiparallel tetramer. Paramagnetic NMR and fluorescence studies revealed the antiparallel orientation. Furthermore, computer simulations and sedimentation equilibrium ultracentrifugation experiments confirmed the formation of a stable tetrameric species. This study thus showed that reversing the amino acid sequence of a hetero coiled coil motif can significantly alter its self-assembly behavior.[5, 14, 18-20] Finally the fusogenity of cholesterol anchored Coil-K and Coil-E_r was compared to our Coil-K/Coil-E_r model system for membrane fusion.

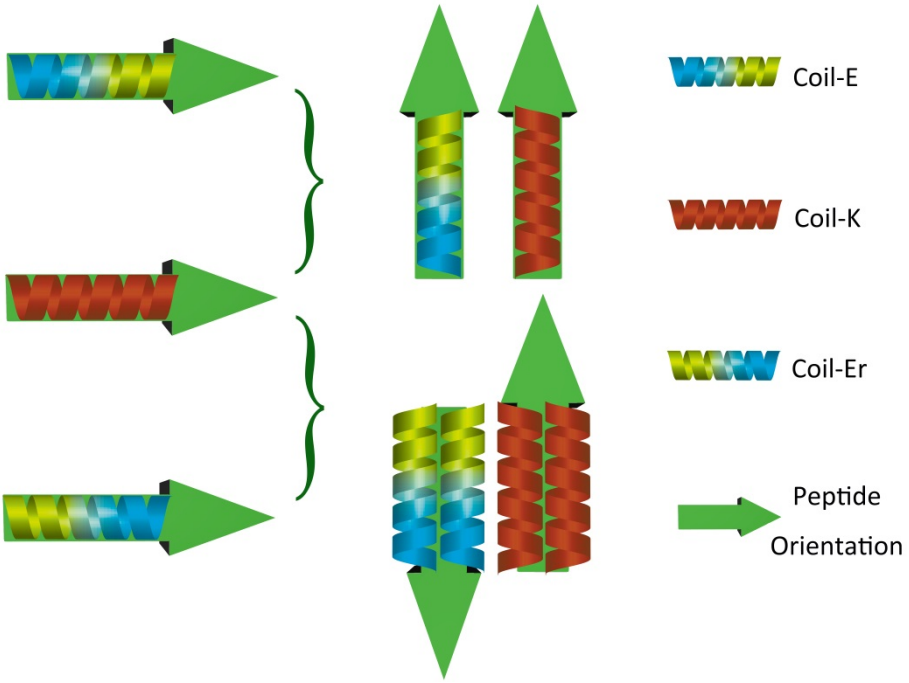

Scheme 1. Schematic representation of Coil-E, Coil-Er and their assembly with Coil-K. The green arrow indicates the orientation of peptide from N terminus to C terminus. An equimolar mixture of Coil-E with Coil-K yields a parallel dimer. An equimolar mixture of peptide Coil-Er with Coil-K yields an antiparallel tetramer.

Experimental Section

Materials.

Fmoc-protected amino acids and Rink Amide resin (0.53 mmol g^{-1}) were purchased from NovaBiochem. HCTU (O-(1H-6-Chlorobenzotriazole-1-yl)-1,1,2,2-tetramethyluronium hexafluorophosphate), HOBT (1-Hydroxybenzotriazole) and DIPEA (N,N-Diisopropylethylamine) were from IRIS Biotech GmbH. NMP (N-methyl-2-pyrrolidone) and DMF (N,N-dimethylformamide) were from Biosolve. DCM (dichloromethane), TFE (2,2,2-Trifluoroethanol), TFE-D_3 (2,2,2-Trifluoroethanol-d_3), and deuterium oxide were obtained from Sigma-Aldrich. Acetic anhydride, piperidine, MeCN (acetonitrile), TFA (trifluoroacetic acid), and TIS (triisopropylsilane) were obtained from Fluka Chemie GmbH. MTSL ((S-(2,2,5,5-tetramethyl-2,5-dihydro-1H-pyrrol-3-yl)methyl methanesulfonothioate) was obtained from Toronto Research Chemicals Inc. PBS buffer

contains: 30 mM K_2HPO4, 19 mM KH_2PO4, 150 mM NaCl, pH=7.4. The pH value was adjusted with either 0.1 M HCl or 0.1 M NaOH. Tris buffer contains 1M tris (2-Amino-2-hydroxymethyl-propane-1,3-diol), pH=7.0.

Peptide Synthesis.

Solid-phase peptide synthesis.

Peptides were synthesized on a CEM-Liberty 1 Single Channel Microwave Peptide Synthesizer using standard Fmoc chemistry.[21] Fmoc-protected Rink amide resin (0.53 mmol g^{-1}) was used to synthesize the peptides on a 0.25 mmol scale. The resin was swollen in DMF for 30 mins before use. Fmoc deprotection was performed using 20% (v/v) piperidine in DMF for 3 mins at 50 W with a maximum temperature of 80 ℃. Four equivalents of a Fmoc-amino acid, four equivalents of HCTU and five equivalents of DIPEA in DMF were used for amino acid coupling for 5 mins at 40 W with a maximum temperature of 80 ℃. For each amino acid coupling cycle, a deprotection and coupling time of 5 and 30 mins were used respectively. For cysteine coupling a cycle comprising 2 mins at 0 W followed by 4 mins at 40 W with a maximum temperature of 50 ^{o}C was used. Two wash steps (1.5 mL DMF) were performed between every amino acid coupling cycle. All peptides were acetylated manually at the N-terminus after completion of the synthesis using 20% (v/v) acetic anhydride in DMF for 1.5 hour. Peptides without a cysteine residue, were cleaved from the resin and side-chain deprotected using a mixture of TFA/water/TIS=95:2.5:2.5 (v/v) for 1 hour.[22] Peptides with a Trt (trityl-) protected cysteine residue were cleaved from the resin with simultaneous side-chain deprotection using TFA/thioanisole/ethandithiol/phenol/H_2O=8.4:0.7:0.5:0.2:0.2 (v/v) for 3 hours at room temperature.[23] The resulting solution was added drop-wise into an excess of 50 ml cold diethyl ether to precipitate the deprotected peptide, followed by centrifugation and the liquid supernatant was removed. This procedure was repeated 3 times with the addition of fresh cold diethyl ether. All the peptides were dried under vacuum, dissolved in MilliQ water and lyophilized yielding a white powder.

MTSL nitroxyl radical label.

MTSL was conjugated to the peptide via a disulfide bond with the cysteine residue. One equivalent peptide (1 mM) was dissolved in 1 M tris buffer (pH=7.0) and five equivalents of MTSL in DMF (50 mM) were added slowly under an argon atmosphere and the final mixture was stirred for 3 hours at room temperature.[24] Next, the samples were lyophilized and stored at -20 ℃ before purification.

Peptide Purification.

The crude peptides were purified by RP-HPLC, using a Shimadzu HPLC system with two LC-8A pumps, and an SPD-10A VP UV-VIS detector. Samples elution was monitored by UV detection at 214 nm and 254 nm. Purification of peptides was performed on a Vydac C18 reversed phase preparative column with a flow rate 15 mL min^{-1}. Peptides were dissolved at a concentration of 5 mg ml^{-1} in a mixture of Acetonitrile/H_2O/tert-butanol=1:1:1 (v/v) and eluted with a linear gradient from B to A. Solvent A=acetonitrile, while solvent B=0.1% TFA in H_2O. Acetylated peptides were purified using a 20 min gradient from 90% to 10% B, with a yield of 30%. MTSL labeled peptides were purified using a 25 min gradient elution from 80% to 20% B, with a typical yield of 20%. Purified peptides were lyophilized and characterized by LC-MS using a Vydac C18 analytical column with a 1 mL min^{-1} flow rate.

Circular Dichroism Spectroscopy.

CD (circular dichroism spectroscopy) spectra were obtained using a Jasco J-815 spectropolarimeter equipped with a peltier controlled thermostatic cell. The ellipticity is given as mean residue molar ellipticity, [θ] (10^3deg cm^2 $dmol^{-1}$), calculated by Eqn (1).[6, 25]

$$[\theta] = (\theta_{obs} \times MRW)/(10 \times lc) \qquad (1)$$

Where θ_{obs} is the ellipticity in millidegrees, MRW is the mean residue molecular weight, l is the path length of the cuvette in cm and c is the peptide concentration in mg/mL.

A 1.0 mm quartz cuvette and a final concentration of 200 μM peptide in PBS (pH=7.4) were used. Spectra were recorded from 250 nm to 200 nm at 25 °C. Unless stated otherwise data points were collected with a 0.5 nm interval with a 1 nm bandwidth and

scan speed of 1nm per second. Each spectrum was an average of 5 scans. For analysis each spectrum had the appropriate background spectrum (buffer or 50% TFE) subtracted.

For determination of the coiled coil thermal dissociation constant, temperature dependent CD spectra were obtained using an external temperature sensor immersed in the sample.[26, 27] The temperature was controlled with the internal sensor and measured with the external sensor. A 10 mm quartz cuvette was used, and the solutions were stirred at 900 rpm. Spectra were recorded from 250 nm to 200 nm, with data collected at 0.5 nm intervals with a 1 nm bandwidth and a scan speed of 1 nm per second. The temperature range was 6 °C to 96 °C with a temperature gradient of 2.0 °C minute^{-1} and a 60 s delay after reaching the set temperature. The spectrum of PBS at 6 °C (average of 5 scans) was subtracted from each spectrum. All the thermal unfolding curves were analyzed using a two-state conformation transition model.[28, 29]

The data was analyzed using a two-state unfolding model to determine the fraction folded using Eqn. (2),

$$F_f = ([\theta] - [\theta]_U)/([\theta]_F - [\theta]_U) \qquad (2)$$

Where $[\theta]$ is the observed molar ellipticity, $[\theta]_U$ is the ellipticity at 222 nm of the denatured state, as determined from the plateau of the ellipticity vs. temperature curve, and $[\theta]_F$ is the ellipticity at 222 nm of the folded state at that temperature as determined from a linear fit of the initial stages of the ellipticity vs. temperature curve.

The fraction unfolded, F_U, was calculated by Eqn. (3),

$$F_U = 1 - F_f \qquad (3)$$

The dimer dissociation constant in the transition zone was calculated using Eqn. (4),

$$K_U = 2P_t F_U^2/F_f \qquad (4)$$

P_t is the total peptide concentration. By taking the derivative of the $\ln(K_U)$ vs. temperature curve and using this in the van't Hoff equation, Eqn. (5), the change in enthalpy associated with unfolding with temperature can be plotted:

$$\Delta H_U = RT^2 \times \frac{d\ln(K_U)}{dT} \qquad (5)$$

The gradient of the enthalpy vs. temperature plot ΔC_p, is the difference in heat capacity between the folded and unfolded forms, and can be used in the Gibbs-Helmholtz equation adapted to monomer-dimer equilibrium, Eqn. (6), to obtain the Gibbs free energy of unfolding as a function of temperature by least-squares fitting,

$$\Delta G_U = \Delta H_m(1 - T/T_m) + \Delta C_p[T - T_m - T\ln(T/T_m)] - RT\ln[P_t] \qquad (6)$$

T_m and H_m are the temperature and enthalpy at the midpoint of the transition at which the fraction of monomeric peptide is 0.5.[9]

^{1}H-magnetic resonance spectroscopy.

To monitor the aromatic region ^{1}H-NMR signals in the range from 6 ppm to 8 ppm of the amino acids W and Y, the peptide amide proton signals were suppressed by proton-deuterium exchange using D_2O. Lyophilized peptide samples were dissolved at a concentration of 0.5 mg ml^{-1} and incubated in D_2O for one hour, followed by lyophilization. This procedure was repeated three times. PBS (10 ml, pH=7.4) was lyophilized and redissolved in D_2O to prepare a PBS/D_2O buffer solution. Peptide samples were prepared with a final concentration of 0.8 mM in PBS/D_2O buffer solution. All ^{1}H-NMR spectra were recorded at 298 K on a Bruker Avance Ⅲ 600 MHz spectrometer with 32 scans for each sample.

Fluorescence spectroscopy.

Fluorescence experiments were conducted on a TECAN Infinite M1000 PRO fluorometer using a 96 well plate. The Z-position was 12500 μm, and the gain was optimized according to the amount of fluorophore in the sample. Excitation and emission slits were set at 5 nm. Emission spectra were measured from 290 nm to 450 nm in 1 nm steps at a fixed excitation wavelength of 275 nm. The temperature was set at 25℃. For consistent mixing, the plate was shaken inside the fluorometer for 30 seconds (2 mm linearly, 70 × per minute). The spectra were corrected by subtraction of PBS or PBS/ TFE=1:1 (v/v) spectra as a background spectrum. The concentration of peptide E or K was 20 μM in each measurement, with 250 μL volume of peptide solution in each well.

Sedimentation Equilibrium Analytical Ultracentrifugation

Sedimentation equilibrium analytical ultracentrifugation measurements were conducted using a Beckamn-Optima XL-I analytical ultracentrifuge fitted with an An-60 Ti rotor. Peptide solutions were prepared in PBS buffer, pH 7.4, at peptide concentrations which gave an initial absorbance in the range 0.2-0.6 A.U. The samples were spun at three speeds

(between 34,000-50,000 rpm) at 20 ^{o}C. The data was then fitted to a single-ideal species model using Ultrascan.[30]

Molecular simulation

All simulations were carried out with the GROMACS molecular dynamics package using the version 2.1 of the MARTINI coarse-grained force field and its extension to proteins.[31-33] Using this model, the association behavior of several proteins in model membranes has been already simulated and the computational results show good agreement with previous atomistic simulations or experiment.[34-36] To characterize the self-assembly process of Coil-E_r and Coil-K peptides, we have performed 20 independent simulations of four peptides (two Coil-E_r and two Coil-K) randomly distributed in solvent (water with Na^+ and Cl^- ions). The starting coarse-gained structures for the Coil-K have been mapped from the 20 atomistic models of the exactly same peptide reported by Hodges group using NMR.[37] The structures for the Coil-E_r were mapped from 20 coordinates frames obtained during atomistic simulation of a generated α-helical peptide in solution. Before carrying out the MD (molecular dynamics) simulations, a steepest descent minimization was performed, followed by relaxation of the solvent (position restrains on the whole peptide) and of the side chain beads (position restraints on the peptide backbone). After this, the system was further simulated without any restraints to allow self-assembly and equilibration of the formed supramolecular structures for at least 40 microseconds. The detailed description of the model and the simulation conditions are given in the appendix.

Results and discussion

Peptide design and Synthesis.

In this study, Coil-K retains its original sequence whilst Coil-E_r was designed with the reversed amino acid sequence from Coil-E (Table 1). Tryptophan (W) and Tyrosine (Y) were attached to the C- terminus of peptide Coil-K and the N- terminus of peptide Coil-E_r respectively to allow for quantification and analytical studies. A glycine was introduced in order to act as a spacer. This results in derivatives Coil-K_W and Coil-$_Y E_r$. To study the orientation of the peptides in coiled coils, the paramagnetic nitroxyl radical was conjugated

to the C-terminus of Coil-K_W by introduction of the MTSL to a cysteine. When MTSL is conjugated to the C-terminus, it yields peptide Coil-K_W^*; whereas on the N-terminus, peptide Coil-$^*K_W$ will be generated. This approach offers the opportunity to investigate the intermolecular self-assembly stoichiometry and the relative peptide orientation by paramagnetic proton NMR and steady state fluorescence measurements.

Table 1. Peptide primary structure and molecular characterization

Peptide Name	**Sequence** (from N to C terminus)	**Molecular weight** (g mol^{-1})	**D(*, W)** [a]	**^{1}H-NMR signal** [b]	**Fluorescence signal** [c]
Coil-K	Ac-(KIAALKE)$_3$-CONH$_2$	2321	N/A	N/A	N/A
Coil-K_W	Ac-(KIAALKE)$_3$G**W**-CONH$_2$	2564	N/A	√	√
Coil-K_W^*	Ac-(KIAALKE)$_3$G**W**C-CONH$_2$ (MTSL)	2854	6.6	×	×
Coil-$^*K_W$	Ac-C(KIAALKE)$_3$G**W**-CONH$_2$ (MTSL)	2854	36.7	√	√
Coil-E	Ac-(EIAALEK)$_3$-CONH$_2$	2324	N/A	N/A	N/A
Coil-E_r	Ac-(KELAAIE)$_3$-CONH$_2$	2324	N/A	N/A	N/A
Coil-$_Y E_r$	Ac-**Y**G(KELAAIE)$_3$-CONH$_2$	2544	N/A	√	√

a. 'D' short for distance, '*' denotes the position of the 'MTSL' spin label and '$_W$' denote for the tryptophan residue, indicating the distance between the MTSL and the tryptophan functional group. Distances between the '*' paramagnetic nitroxide and the tryptophan play a decisive role in both the NMR and fluorescence signal of '$_W$'. Within 10.5 Å, the NMR signal of W will get totally suppressed while its fluorescence signal gets quenched.[38-48] b Refers to 1D-proton NMR chemical shifts from 6-8 ppm. c Refers to fluorescence emission spectra from 285-445 nm with excitation at 275 nm. Both NMR and fluorescence measurements were performed in presence of pH=7.4 PBS buffer. '√' indicates there is signal observed while '×' indicates there is no signal observed.

All peptides were synthesized by standard Fmoc solid phase synthesis on Rink Amide resin and further purified by C18 RP-HPLC. Peptides were identified using LC-MS mass spectrometry and analytical HPLC results confirm that the purity of the peptides is higher than 99% (See Appendix Figure A2-A4).

Circular Dichroism spectroscopy

Circular dichroism spectroscopy was used to study the secondary structure of the peptides. Both Coil-K and Coil-Er show α-helical structures with two minima at 222 nm and 208 nm wavelength in phosphate buffered saline (PBS, pH=7.4) at room temperature. The equimolar mixture shows typical coiled-coil characteristics with the [θ]222/[θ]208 ellipticity ratio > 1 (Figure 1A).[49] To further investigate the peptide secondary structure, TFE was added. TFE is known to enhance intramolecular α-helicity while disrupting any intermolecular interactions (i.e. coiled coil assemblies).[50] Comparison of the [θ]222/ [θ]208 ellipticity ratio and α-helix values before and after TFE addition showed that in both peptides Coil-K and Coil-Er, the [θ]222/[θ]208 ellipticity ratio and α-helix values increases, indicative of monomeric α-helices. In contrast, for the equimolar peptide complex CC-K/Er, both the ellipticity ratio and helicity decreased, indicating the disturbance of intermolecular coiling, affirming the existence of coiled coils (Table 2).[51]

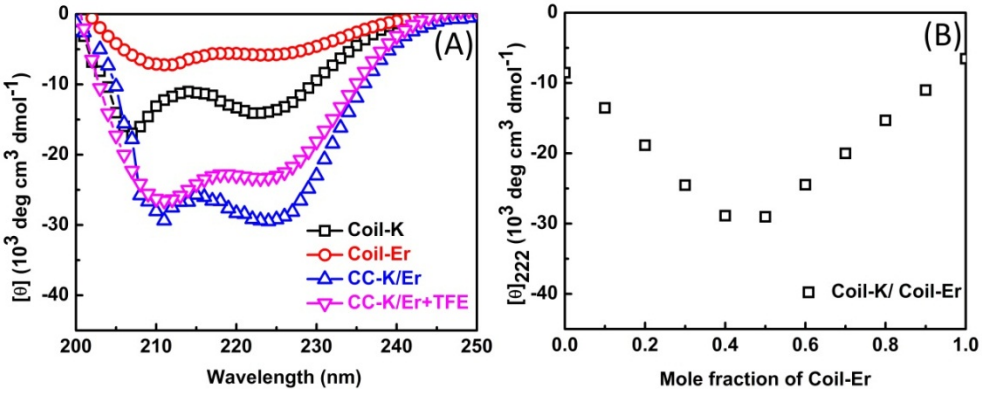

Figure 1. Circular dichroism spectra of peptide Coil-K, Coil-Er and their 1:1 mixture. (A) Secondary structures of peptide Coil-K, Coil-Er and their equimolar mixture CC-K/Er in pH=7.4 PBS buffer, as well as CC-K/Er in TFE/PBS=1:1 (v/v) solution. (B) Binding stoichiometry of the peptide Coil-K and Coil-Er. Mean residue molar ellipticities at 222 nm wavelength for mixtures of the Coil-K and Coil-E peptides as a function of the mol fraction of the Coil-E peptide. [Total peptide]= 200 μM, PBS, pH=7.4, 25 ℃.

Furthermore, CD spectra were also used to determine the coiled coil binding properties. First the Coil-K and Coil-E_r binding stoichiometry was measured using a Job-plot by changing the ratio of the mole fraction between Coil-K and Coil-Er, while keeping the total

peptide concentration constant at 200 μM (i.e. Plotting $[\theta]_{222}$ as a function of the mole fraction of Coil-E_r). A minimum molar ellipticity at $[\theta]_{222}$ was observed when Coil-K and Coil-E_r were mixed with equimolar amounts, indicative of a 1:1 stoichiometry (Figure 1B).

Table 2. Secondary and quaternary CD spectroscopic data of CC-K/Er.

Peptide [a]	$[\theta]_{222}$		% α-helix [b]		$[\theta]_{222}/[\theta]_{208}$		Coiled-Coil[c]
	Benign	50% TFE	Benign	50% TFE	Benign	50% TFE	
Coil-K	-14105	-19965	45	64	0.82	0.85	-
Coil-E_r	-5758	-16476	18	53	0.83	0.85	-
CC-K/E_r	-29163	-23280	93	75	1.13	0.87	+

[a] CC-K/E_r refers to an equimolar concentration of Coil-K and Coil-E_r. [b] The percentage of α-helicity is calculated from 100 times the ratio between observed $[\theta]_{222}$ and predicted $[\theta]_{222}$ for an α-helical peptide of n residues. The predicted α-helicity is determined from the formula: $[\theta]_{222}$=-40000×(1-4.6/n). [52, 53c] The signal + signifies a significant decrease in the $[\theta]_{222}/[\theta]_{208}$ ratio from PBS to 50% TFE in PBS, indicative of the folded coiled-coil structure and vice versa. [Total Peptide]=200 μM, PBS, pH=7.4, 25℃.

Next, the thermal stability of CC-K/E_r was determined by plotting the molar ellipticity at 222 nm as a function of temperature.[6,52] The transition showed to be reversible (Figure 2).

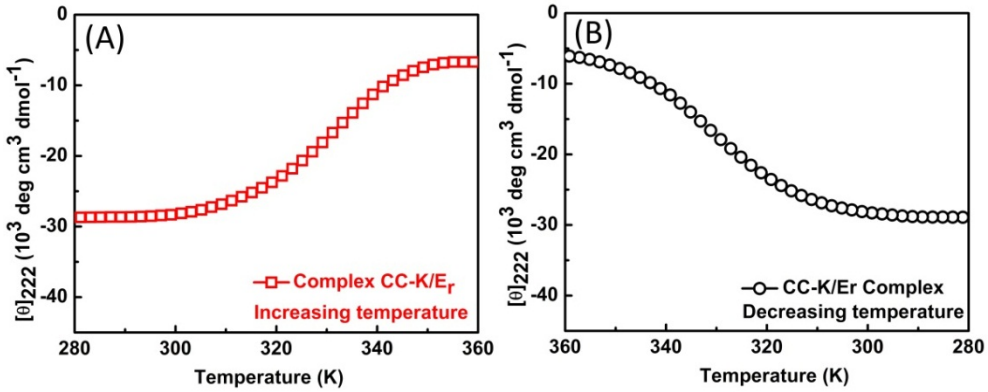

Figure 2. The thermal dissociation and association curves of CC-K/E_r, indicated by the temperature dependent value of $[\theta]_{222}$. (A) Reveals decreasing absolute values of $[\theta]_{222}$ due to the disassembly of the CC-K/E_r complex by temperature increase. (B) Reveals increasing absolute values of $[\theta]_{222}$ due to the assembly of the CC-K/E_r complex by temperature decrease. [Total peptide]= 40 μM, PBS, pH=7.4.

CC-K/E_r showed to have a two-state transition from 100% folded to 0% folded. The T_m was determined from the unfolding curve to be 58 ^oC (Figure 3A). The enthalpy of the temperature dependent unfolding curve was calculated from the Van't Hoff plot (Figure 3B). For the CC-K/E_r complex, the enthalpy value increases linearly with rising temperature, which is the expected behavior for a two-state transition (Figure 3C). [40] The gradient of the enthalpy-temperature curve is the heat capacity between the folded complex state and the unfolded monomer state.[54] The positive value (0.26 kcal mol^{-1} K^{-1}) of the heat capacity indicates that nonpolar surfaces are exposed to water during dissociation of the coiled coil complex.[55] Using the heat capacity value, the change in free energy of unfolding at different temperatures was calculated to be 9.6 kcal mol^{-1} (Figure 3D). This is similar to the original CC-K/E (See Appendix Figure A5). The dissociation constant at 25 ^oC associated with this ΔG^{H_2O} value is 6.4×10^{-8} M. This value is close to the reported 7.0×10^{-8} M for CC-K/E (Table 3).[25]

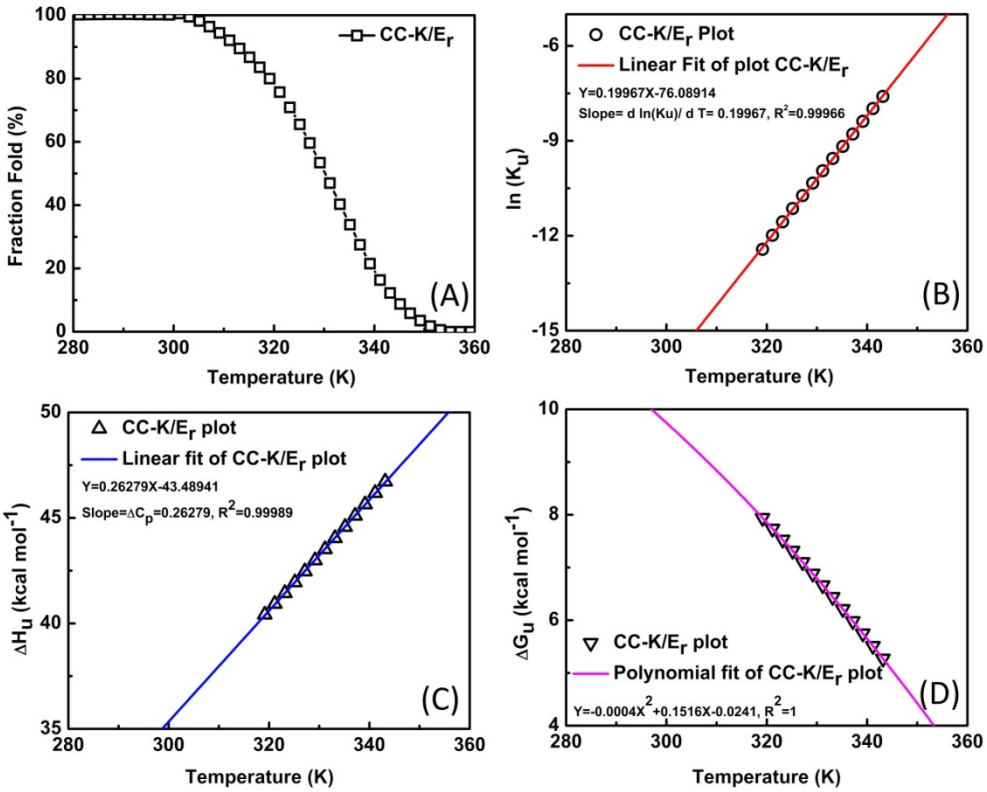

Figure 3. Thermal unfolding properties of CC-K/E_r. (A) Thermal dissociation curve of coiled coil complex CC-K/E_r. Melting temperature is 331 K (58 ^oC). (B) Van't Hoff plot of

the thermal denaturation of CC-K/E_r. The dissociation constant at 25 °C is $K_u = 6.4 \times 10^{-8}$ M. (C) Shows the linear dependence of the enthalpy of unfolding of CC-K/E_r on temperature. (D) Describes the free energy associated with the unfolding of CC-K/E_r as a function of temperature. The least-squares fit gives a ΔG^{H_2O} value at 25 °C of 9.6 kcal/mol. [Total peptide]= 40 μM, PBS, pH=7.4.

Table 3. Coiled coil dissociation constant measured from CD spectroscopy.

Coiled-coil Complex	T_m (°C) [b]	ΔG_u (kcal mol^{-1}) [c]	K_d (M) [d]
CC-K/E [a]	58	9.6	7×10^{-8}
CC-K/E_r	58	9.6	6.4×10^{-8}

[a] data taken from literature and we further confirmed by repeating the measurements (See Appendix).[5, 6] [b] T_m = melting temperature, at which 50% of the coiled coil complex was dissociated. [c] Gibbs free energy of unfolding at 25℃. [d] K_d = the dissociation constant.

Comparison of the CD spectra of CC-K/E and CC-K/Er did not show any significant differences. Remarkably, the binding energy was almost identical. To this point, CC-K/E and CC-K/Er showed to behave similarly.

^{1}H-proton NMR spectroscopy

600 MHz 1H-nuclear magnetic resonance spectroscopy was used to study the orientation and assembly stoichiometry of the coiled coil scaffold CC-K/Er. Paramagnetic NMR spectroscopy was used to investigate the peptide quaternary structure. With this method, one can easily recognize the complementary coiled coil peptide orientation and assembly stoichiometry of the complex by determining whether suppression of the peptide specific proton signals due to the paramagnetic relaxation enhancement (PRE) effect. [56]

For this, the peptides need to have a functional group with a characteristic NMR signal and one of the peptides is modified with a signal suppressing paramagnetic spin label. In this study, Tryptophan (W) and Tyrosine (Y) were used to label the C- terminus of Coil-K and the N- terminus of Coil-Er respectively, as the characteristic aromatic signals are well separated from the other signals (i.e. Coil-K_W and Coil-$_Y$Er). In addition, the paramagnetic spin label MTSL was introduced onto either the N- or the C-terminus of Coil-KW, yielding Coil-*K_W or Coil-K_W*. To avoid spectral overlap of the aromatic protons with N-H amide protons, the latter were suppressed by 'H-D exchange' before each NMR experiment.

The aromatic region of tryptophan (W) has four multiplets while tyrosine (Y) shows two doublets within the 6 to 8 ppm range. Peptide Coil-K_W* shows full suppression of the

tryptophan signals (Figure 4). This is due to the MTSL nitroxide PRE effect. PRE suppression only occurs when a nucleus is in close proximity with the paramagnetic center (< 13 Å), and full suppression occurs within a 10.5 Å radius.[46] In peptide Coil-K_W*, the average distance between the tryptophan aromatic protons and the nitroxyl radical is 6.6 Å, resulting in suppression of the aromatic protons. In contrast, in peptide Coil-*K_W the average distance between the aromatic protons and the nitroxyl radical is 36.7 Å and therefore no PRE effect is observed (Figure 4) (All the distances were calculated using Hyperchem).

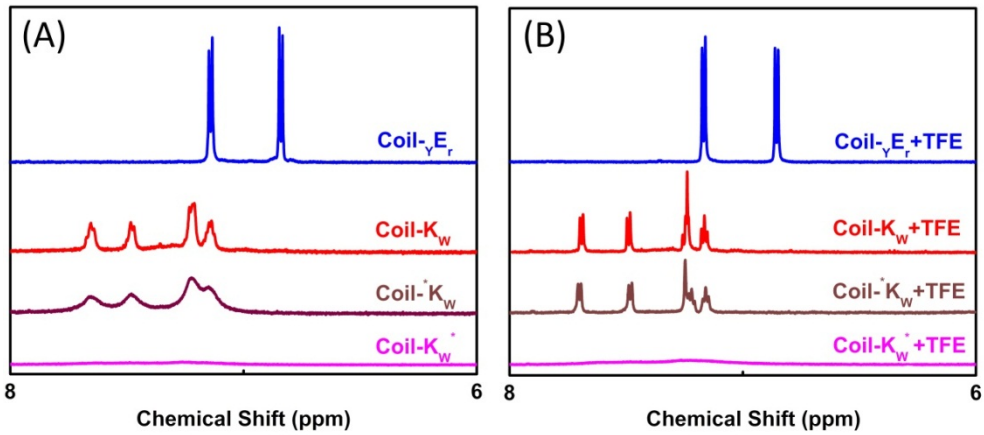

Figure 4. Aromatic region (6-8 ppm) of 600 MHz ^{1}H-nuclear magnetic resonance spectra showing tryptophan indole and tyrosine hydroxyphenyl functional groups of Coil-K and Coil-E derivatives respectively. (A) The aromatic signal of Coil-$_Y$E$_r$, Coil-K_W, Coil-$^*K_W$ and Coil-K_W^* in PBS buffer. (B) The aromatic signal of single peptides in the presence of 50% TFE in PBS buffer. [Total peptide]= 0.8 mM, 25 ^{o}C.

An equimolar mixture of peptide Coil-K_W and Coil-$_Y$E$_r$ and their MTSL labeled variants were studied in PBS at room temperature to obtain information regarding the relative peptide orientation (Figure 5). When the peptides are assembled into coiled coils, the characteristic knobs-into-holes packing leads to the close distance of the peptides identical termini, but the distance of the opposite termini is too large for the PRE effect (length of Coil-K = 37.1 Å).[37] Thus the PRE effect can be used to determine the peptide orientation during self-assembly of the coiled coil. It is obvious that the tyrosine aromatic signals in Coil-$_Y$E$_r$, only gets suppressed when an antiparallel orientation is adopted in coiled coil formation with Coil-K_W^*. This was indeed observed (Figure 5). Recovery of the tyrosine signal was obtained upon the addition of 50% TFE due to disassembly of the coiled coil.

This strongly suggests that peptide Coil-K_W and Coil-$_YE_r$ form an antiparallel coiled coil motif. An equimolar mixture of Coil-$^*K_W$ and Coil-$_YE_r$ did not show suppression of the tyrosine signal, thereby supporting the antiparallel orientation (Figure 5).

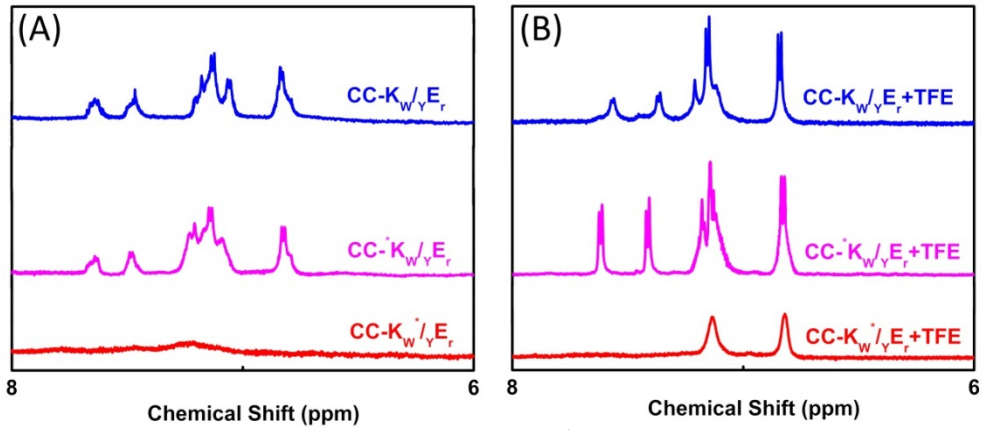

Figure 5. Aromatic Region (6-8 ppm) of 600 MHz ^{1}H-nuclear magnetic resonance spectra showing tryptophan indole and tyrosine hydroxyphenyl functional groups of equimolar mixtures of Coil-K and Coil-E (short name CC-K/E). (A) Aromatic signals of peptide CC-K/E complex in PBS. Blue line indicates CC-$K_W/_YE_r$, pink line indicates CC-$^*K_W/_YE_r$ and red line indicates CC-K_W*$/_YE_r$. (B) Aromatic signals of CC-K/E in 1:1 (v/v) TFE: PBS. Blue line indicates CC-$K_W/_YE_r$, pink line indicates CC-*$K_W/_YE_r$ and red line indicates CC-$K_W^*/_YE_r$. [Total peptide]= 0.8 mM, PBS, pH=7.4, 25 ^{o}C.

Next, the stoichiometry of Coil-K and Coil-$_YE$ coiled coil formation was investigated by paramagnetic NMR. First, Coil-K_W^* and Coil-$_YE_r$ were mixed in a 2:1 molar ratio (Figure 6). Here the tyrosine aromatic proton signals are fully suppressed. This was also observed for the equimolar mixture. However, when Coil-K_W^* and Coil-$_YE_r$ were mixed in 1:2 molar ratio, tyrosine aromatic protons were observed. This is indicative that there is an excess of Coil-$_YE_r$ which is not suppressed. This shows that Coil-K and the reverse sequence Coil-E_r bind approximately in a 1:1 stoichiometry.

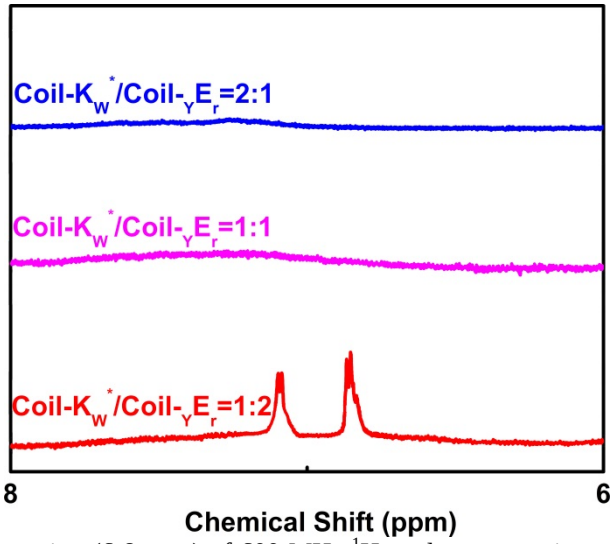

Figure 6. Aromatic region (6-8 ppm) of 600 MHz ^{1}H-nuclear magnetic resonance spectra showing tyrosine hydroxyphenyl functional groups of different molar ratio mixtures of Coil-K_W^* and Coil-$_Y$E$_r$. (A) From top to bottom, the molar ratio between Coil-K_W^* and Coil-$_Y$E$_r$ is 2:1, 1:1 and 1:2 respectively. [Total peptide]=0.8 mM, PBS, pH=7.4, 25 ^{o}C.

Steady state fluorescence spectroscopy

To confirm the relative peptide orientation in the coiled coil, steady state fluorescence spectroscopy studies were performed using FRET (fluorescence resonance energy transfer) or fluorescence quenching assays. The fluorescence emission spectra of the individual peptides are shown in Figure 7. Typical spectra were obtained except for Coil-K_W^*, due to the presence of spin label in the vicinity of the tryptophan (vide infra).

FRET only occurs when the donor and acceptor are within the Förster Distance (≈ 1 nm).[57] When a mixture of Coil-$_Y$E$_r$ and Coil-K_W forms coiled coils with an antiparallel orientation, FRET between the donor tyrosine and the acceptor tryptophan is expected. Indeed, FRET was observed using an excitation wavelength of 275 nm. From the emission spectra in Figure 8A, it is noticeable that when an equimolar mixture of Coil-K_W and Coil-$_Y$E$_r$ is used, the Coil-K_W fluorescence intensity increases while the Coil-$_Y$E$_r$ fluorescence intensity decreases due to the FRET phenomenon leading to the energy transfer from the donor Y to the acceptor W. This confirms the small distance between the N-terminus of peptide Coil-$_Y$E$_r$ and the C-terminus of peptide Coil-K_W, implying an antiparallel orientation of CC-K_W/$_Y$E$_r$. Upon the addition of 50% TFE, the coiled coil dissociates, which led to an

increase of tyrosine fluorescence, and a decrease of tryptophan fluorescence. Thus addition of TFE leads to a loss of FRET due to disassembly of the antiparallel coiled coil of Coil-K and Coil-E_r.

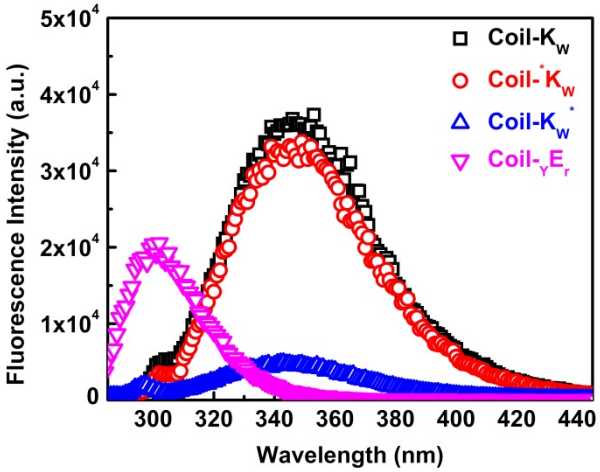

Figure 7. Fluorescence emission spectra of W and Y on peptide Coil-K_W and Coil-$_YE_r$ and their derivatives are shown with excitation at 275 nm. [Total peptide]= 50 μM, PBS, pH=7.4, 25 ^oC.

This FRET assay strongly suggests an antiparallel orientation of the peptides in the coiled coil, but it might not be accurate enough to distinguish between dimeric or multimeric assemblies.

Therefore a fluorescence quenching assay was performed. In fluorescence spectroscopy measurements, the fluorophore electron excited singlet state will be quenched when a stable nitroxyl radical is within a distance of 12 Å due to an electron exchange interaction.[39, 41, 58-63] For example, tryptophan fluorescence is quenched in peptide Coil-K_W^*, as the distance to the nitroxyl radical of the MTSL label is shorter than 12 Å; while in peptide Coil-$^*K_W$ no quenching is observed as the distance between the nitroxyl radical and tryptophan is longer than 12 Å (Figure 7) .

Here, peptide Coil-K_W^* and peptide Coil-$_YE_r$ were utilized to confirm the antiparallel orientation of the peptides in CC-K/E_r. In an equimolar mixture of these two peptides, the fluorescence signal of Coil-$_YE_r$ is quenched (Figure 8B). Addition of 50% TFE resulted in the dissociation of the coiled coil. As a result, the distance between Coil-K_W^* and Coil-$_YE_r$ increases, and the tryptophan fluorescence was observed. These findings further proof that the CC-K/E_r coiled coil motif has indeed an antiparallel orientation.

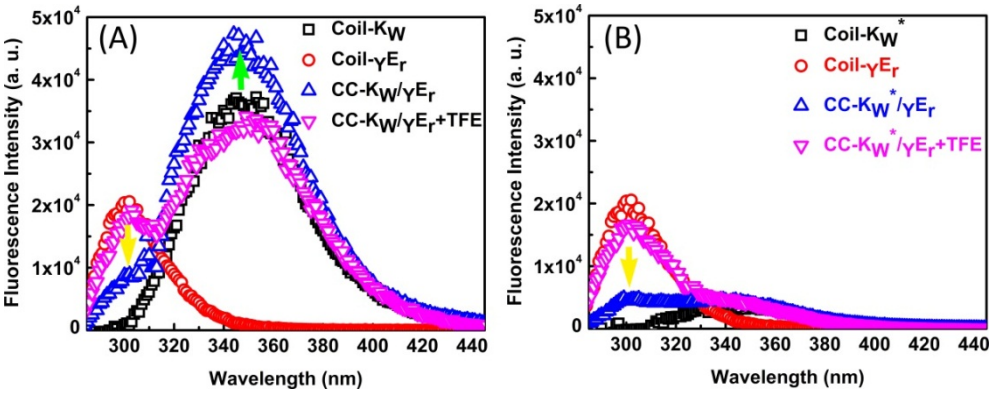

Figure 8. Fluorescence emission spectra of W and Y on single peptides and in the coiled coil complex are shown with excitation at 275 nm. (A) presents the fluorescence spectra of Coil-K_W and Coil-$_YE_r$, and their equimolar mixture emission FRET spectra in PBS buffer as well as emission spectra in TFE/ PBS=1:1 (v/v). The green arrow indicates the signal increase of W and the yellow arrow indicates the signal decrease of Y. (B) presents the single peptide fluorescence spectra of Coil-K_W^* and Coil-$_YE_r$, and their equimolar mixture emission quenching spectra in PBS buffer as well as emission spectra in TFE/ PBS=1:1 (v/v). The yellow arrow indicates the signal decrease of Y. [Total peptide]=50 μM, 25 ^oC.

In summary, FRET and fluorescence quenching experiments show strong evidence for the antiparallel peptide orientation in the CC-K/E_r coiled coil motif. This result further supports the finding of the paramagnetic NMR study.

Sedimentation Equilibrium

To determine the oligomer state of the CC-K/Er species in solution, sedimentation equilibrium measurements were performed using ultracentrifugation (AUC). Datasets were fitted to a single-ideal species model using Ultrascan and the average mass of the species was determined to be 10,620 Da, with 95% confidence limits (determined by Monte Carlo analysis) to be +57 Da, -64 Da. There are no systematic residuals for the fitting. Hence, weight-averaged molecular weights typical of a tetramer for CC-K/Er were observed.

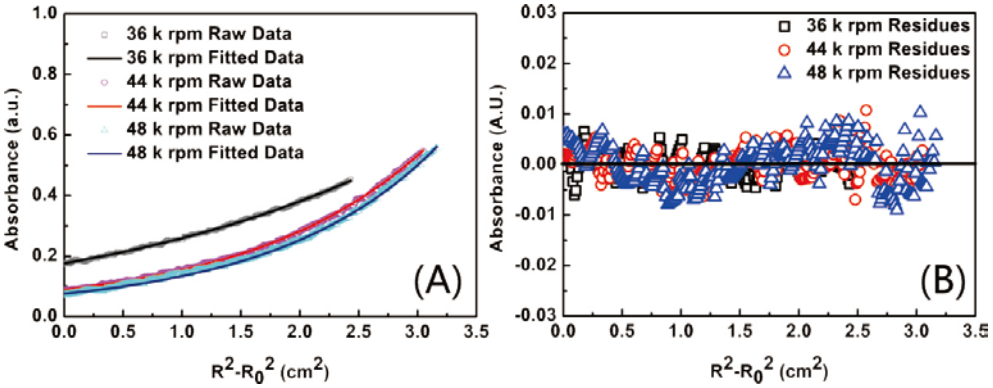

Figure 9. AUC (analytical ultracentrifugation) data for the CC-K/Er species (A) and residuals (B).

Molecular simulation

All the experimental data has shown so far that in an equimolar mixture of Coil-K and Coil-E_r, coiled coils are only formed with an antiparallel orientation of the peptides. However, the exact arrangement of the peptides within this tetramer is still unknown. To have further information about the peptide orientation of the peptides within the tetramer, molecular simulations were performed. In all the simulations, the randomly distributed peptides (two Coil-K and two Coil-E_r) spontaneously aggregated into supra-molecular structures. The four peptides first came into contact, and then orientate parallel to each other forming a 4-helix-bundle with a hydrophobic core. The aggregation process itself is relatively fast, approximately 0.5 microseconds, while 20 to 40 microseconds are needed for equilibration (each peptide rotation around its own axis or flipping to optimize the core). After equilibration, each peptide makes two longitudinal interfaces with two neighboring peptides, and the final cylinder is ~2.5 nm in diameter and the height.

All the possible tetramer configurations can be classified in two major classes: (1) having four K-Er interfaces or (2) having two K-Er interfaces, together with one K-K and one Er-Er interface. Likewise all the formed interfaces may be in parallel or in antiparallel orientation. This gives eleven distinct possible conformations for the obtained tetramers.

Our self-assembly simulations show two possible tetramer structures with high forming probability and stability: one with two K-E_r interfaces and the other with four K-E_r

interfaces. Both of these complexes have antiparallel orientations between Coil-K and Coil-E_r helices, but the two copies of both Coil-K and Coil-E_r are taking parallel orientations (Figure 10).

These simulations compliment the experimental techniques by providing information about binding motifs or conformations in the tetramers. As these binding conformations in solution are currently inaccessible for experimental imaging techniques, this is an important result. To decisively determine the most stable conformations by CGMD (coarse grained molecular dynamics), the systems should be equilibrated for considerably increased timescales and/or free energies should be extracted for all eleven possible conformations. Before such an effort is undertaken, one should judge whether the additional insight gained by such a study outweighs the huge computational investment required for such an analysis. Supported by our well-chosen computational setup, i.e. avoiding a bias in the starting conditions, and the observation of a complete reorientation event within simulation time for the heterodimer case, we are confident to conclude that the most probable binding conformations are indeed sampled by our CGMD simulations. Thus, this simulation showed unequivocally that Coil-K and Coil-E_r assemble in a tetramer only, which is in line with the sedimentation equilibrium study.

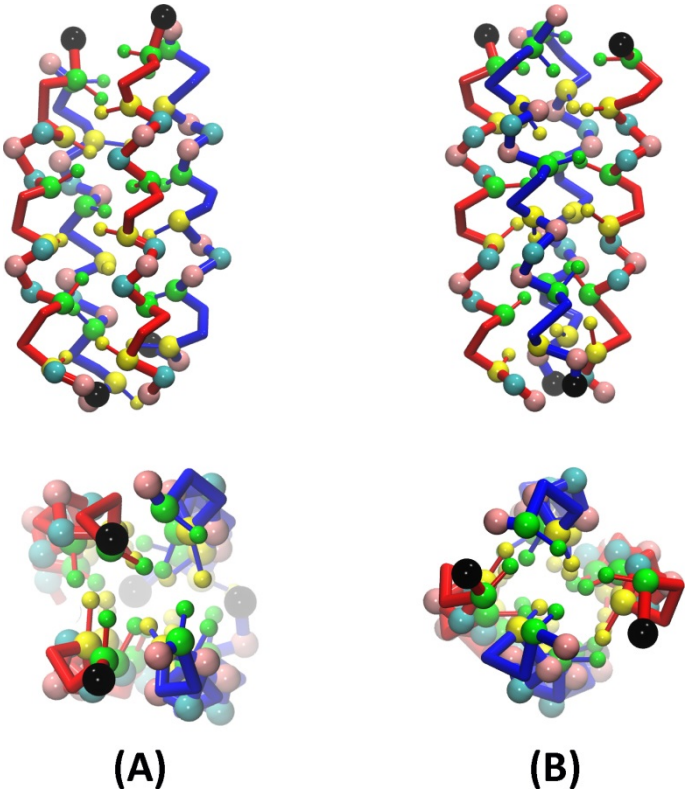

Figure 10. Two possible CC-K/E_r tetramer configurations resulting from molecular dynamics simulations. Up is the lateral view and down is the top view. (A) shows CC-K/Er antiparallel tetramer with two K-Er interfaces. (B) shows CC-K/Er antiparallel tetramer with four K-Er interfaces.

Liposome fusion study

By using various analytical techniques it has been demonstrated that combining peptides Coil-K and Coil-E_r leads to the formation of anti-parallel tetrameric coiled coils, whereas peptides Coil-K and Coil-E form parallel dimeric coiled coils. Remarkably, these two peptide pairs have a similar binding energy. Once incorporated into liposomal membranes, peptides Coil-K and Coil-E have shown to induce efficient and targeted membrane fusion.[6] Here the contest of the aggregation state and orientation vs. binding energy of the coiled coil complexes on the ability to induce membrane fusion was investigated (Scheme 2). For this reason, fusogenic peptides were synthesized which consist of three distinct segments: 1)

the peptide segment, which serves as the recognition unit, 2) a hydrophobic anchor, which enables the stable anchoring of the peptides into liposomal membranes and 3) a hydrophilic spacer, which supplies the peptides with the ability to reorient in order to form coiled coil motifs efficiently.[13] The peptide segment consisted of Coil-K, Coil-E or Coil-E_r, whereas the anchor was constituted by cholesterol and the spacer by 12-polyethylene glycol (PEG_{12}). The resulting lipidated peptides are denoted CPK, CPE and CPE_r. Peptide decorated liposomes were prepared (lipid composition: DOPC/DOPE/CH, 2/1/1 molar ratio and 1 mol% lipidated peptide) by mixing appropriate amounts of lipid and lipidated peptide stock solutions (in $CHCl_3$ and $CHCl_3$/MeOH 1/1 respectively), evaporating the solvent, addition of PBS buffer (yielding a total lipid concentration of 0.1 mM) and sonication for 1 minute at 50°C. A typical fusion experiment was performed by combining equimolar amounts of Coil-K decorated liposomes with Coil-E or Coil-E_r decorated liposomes. The characterization of the fusion events was performed by optical density measurements and DLS, as well as lipid and content mixing assays.

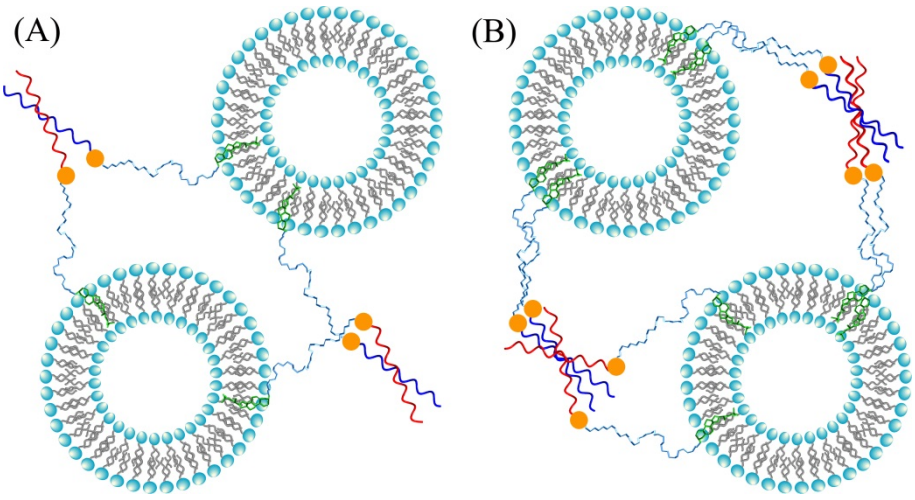

Scheme 2. Schematic diagram of liposome fusion. (A) zipper like fusion model: parallel dimeric coiled coil induced liposome fusion, the blue helix indicates the Coil-E peptide. (B) Non-zipper like fusion model: antiparallel tetrameric coiled coil induced liposome fusion, the blue helix indicates the Coil-E_r peptide. Common symbols: light blue bilayer vesicle=liposome; red helix=Coil-K; green anchor=Cholesterol; light blue linker=PEG12; orange dot=peptide N-terminus.

Upon combining Coil-K decorated liposomes with Coil-E (or Coil-E_r) decorated liposomes, an increase in particle size is expected due to coiled coil formation. The particle size increase can reflect fusion events and/or aggregation and was determined by measuring the optical density of the mixed liposomes at λ=400 nm. A rapid increase in size was observed for both vesicle combinations (equimolar amount of CPK-liposome with CPE-liposome or with CPE_r-liposome), which indicates that both coiled coil motifs are formed efficiently (Figure 11A).

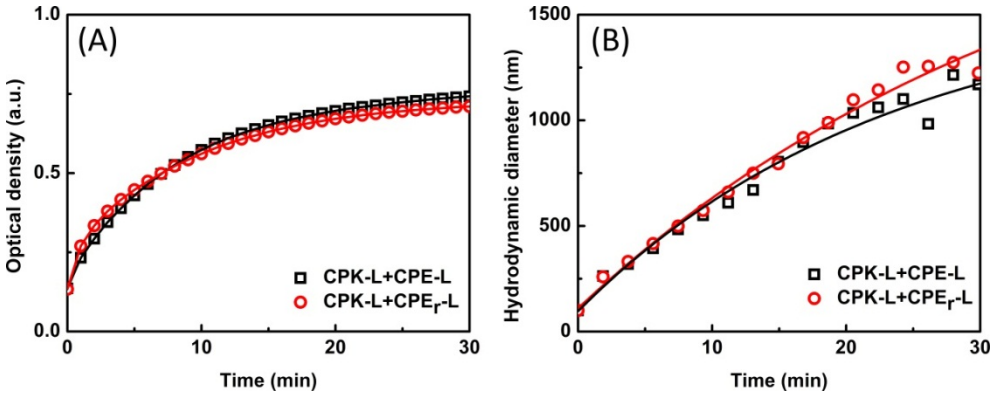

Figure 11. (A) Optical density measurements at λ=400 nm. (B) Dynamic light scattering of liposome fusion size increasing. Black line shows plots of equimolar mixture of Coil-K decorated liposome with Coil-E decorated liposome, while red line shows plots of equimolar mixture of Coil-K decorated liposome with Coil-E_r decorated liposome. Liposome concentration is 0.25mM with 1% peptide decoration. All the measurements were done in PBS, pH 7.4, at 25 ^oC.

DLS measurements confirmed these results and indicated that aggregates of particles >1 μm were formed (Figure 11B). Next, lipid mixing experiments were performed to investigate the extent to which both coiled coil motifs were able to induce lipid mixing. For this assay, a FRET pair was incorporated in the membrane of the Coil-K decorated liposomes (donor: DOPE-NBD and acceptor: DOPE-LR). Upon lipid mixing of these Coil-K liposomes (CPK-L) with Coil-E liposomes (CPE-L) or Coil-Er liposomes (CPE_r-L), the average distance between donor and acceptor increases, giving rise to an increase in donor emission. The donor emissions were continuously measured for 30 minutes and the results show no notable differences between parallel and anti-parallel coiled coil formation, both coiled coil orientations are able to induce fusion between liposomes in an efficient manner (Figure 12A).

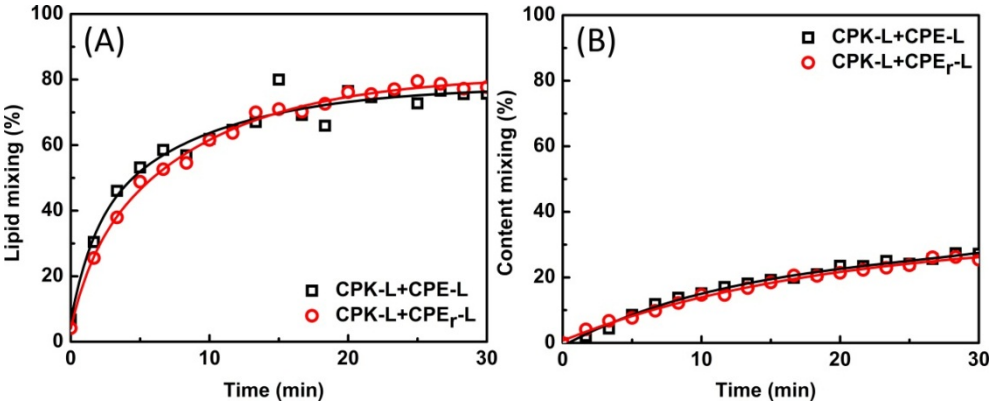

Figure 12. (A) Fluorescence traces showing lipid mixing between fluoresecence (NBD/LR) labeled CPK liposomes with non-fluoresence labeled CPE or CPE_r liposomes. (B) Content mixing between non-fluorescent CPK liposomes with sulforhodamine labelled (20mM) CPE or CPE_r liposomes. Black line shows plots of equimolar mixture of CPK liposomes with CPE liposomes, while red line shows plots of equimolar mixture of CPK liposomes with CPE_r liposomes. Liposome concentration is 0.1 mM with 1% peptide. All the measurements were performed in PBS, pH 7.4, at 25 ^oC.

However, full fusion is defined as lipid and content mixing and therefore we proceeded by performing a content mixing assay. Here, Coil-E or Coil-E_r decorated liposomes were loaded with sulforhodamine B at a self-quenching concentration of 20 mM. Content mixing of these Coil-E or Coil-Er decorated liposomes with the non-fluorescent Coil-K liposomes decreases the concentration of sulforhodamine B, which results in relief of self-quenching and an increase in fluorescence intensity (Figure 12B). Consistent with the lipid mixing experiments, no significant difference in content mixing was observed between both coiled coil motifs, both orientations and oligomer states induce efficient content mixing. This indicates that for this peptide mediated fusion system, the coiled coil binding energy plays an important role and not its aggregation state or the relative peptide orientation.

Conclusion

Reversing the peptide sequence of Coil-E yields Coil-E_r which in the presence of equimolar amounts of Coil-K, results in the formation of an antiparallel tetrameric coiled coil and not an antiparallel heterodimeric coiled coil. This shows that reversing the peptide

sequence significantly alters the assembly behavior, which is in line with previous studies on proteins.[5, 6, 37, 51]

Remarkably, the binding energy is similar but the oligomer state and relative peptide orientation are different. This study shows that reversing the amino acid sequence in a heterodimeric parallel coiled coil motif significantly alters its self-assembly property and one cannot assume that it yields an antiparallel heterodimer, as previously reported.[12, 64] This study demonstrates that a coiled coil assembly is sensitive to small changes and care should be taken when redesigning the amino acid sequence of known coiled coil structures. In addition, this study offers a new coiled coil candidate for the reduced SNARE induced membrane fusion model study. Cholesterol modified peptide Coil-K and Coil-E_r induced liposome fusion comparable to the Coil-K and Coil-E induced liposome fusion. This suggests that in this peptide mediated membrane fusion system, the coiled coil binding energy is a more decisive factor while the peptide orientation and oligomer state is not.

Appendix

Part 1. Non-zipper like liposome fusion model.

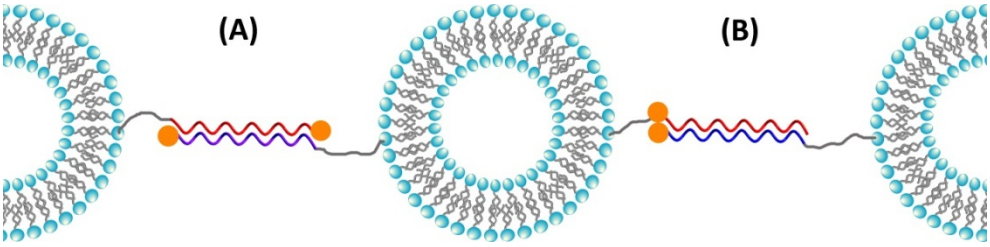

Figure A1. Schematic diagram of (A) Diederichsen and (B) Kros non-zipper like liposome fusion model. Red helix indicates peptide Coil-K ($[KIAALKE]_3$), purple helix indicates peptide Coil-E_r ($[KELAAIE]_3$), blue helix indicates peptide Coil-E ($[EIAALEK]_3$). The orange ball indicates the peptide N-terminus.

Part 2. Mass spectra of the peptides

LC-MS spectra of all the purified peptides are shown below (Figure A 2-4).

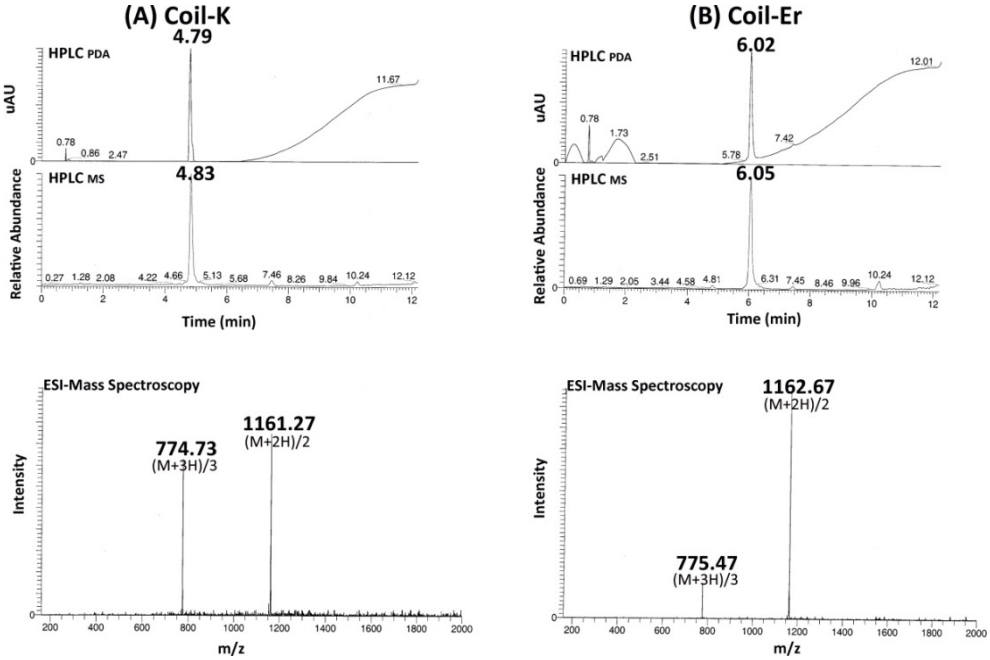

Figure A2. (A) LC-MS spectra of purified Coil-K, (B) LC-MS spectra of purified Coil-E_r. From top to bottom: UV (ultraviolet-visible) spectrum, ESI (electrospray ionization) spectrum, and mass spectrum.

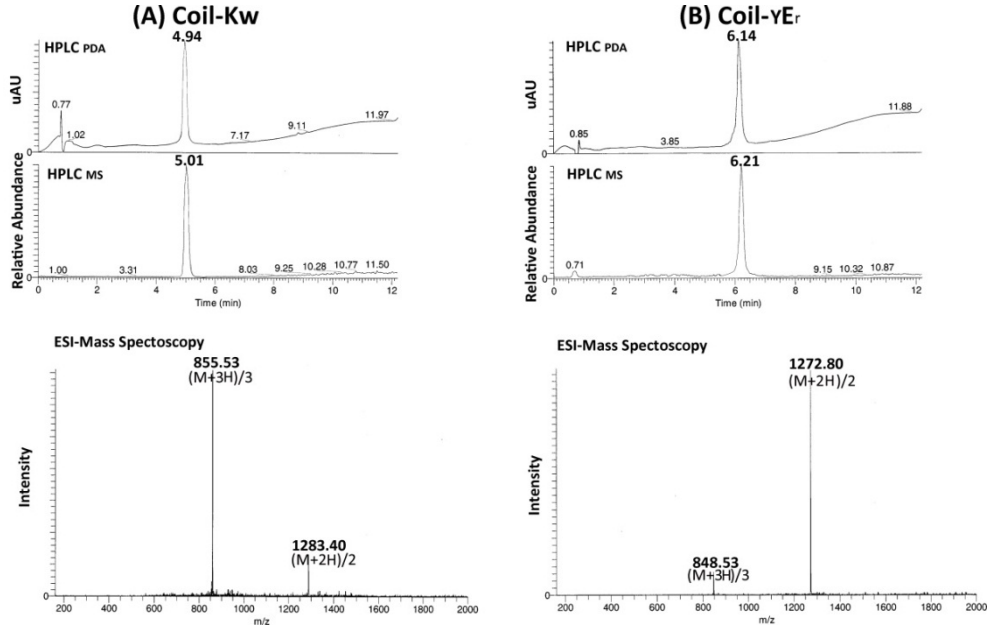

Figure A3. (A) LC-MS spectra of purified Coil-K_W, (B) LC-MS spectra of purified Coil-$_Y E_r$. From top to bottom: UV (ultraviolet-visible) spectrum, ESI (electrospray ionization) spectrum, and mass spectrum.

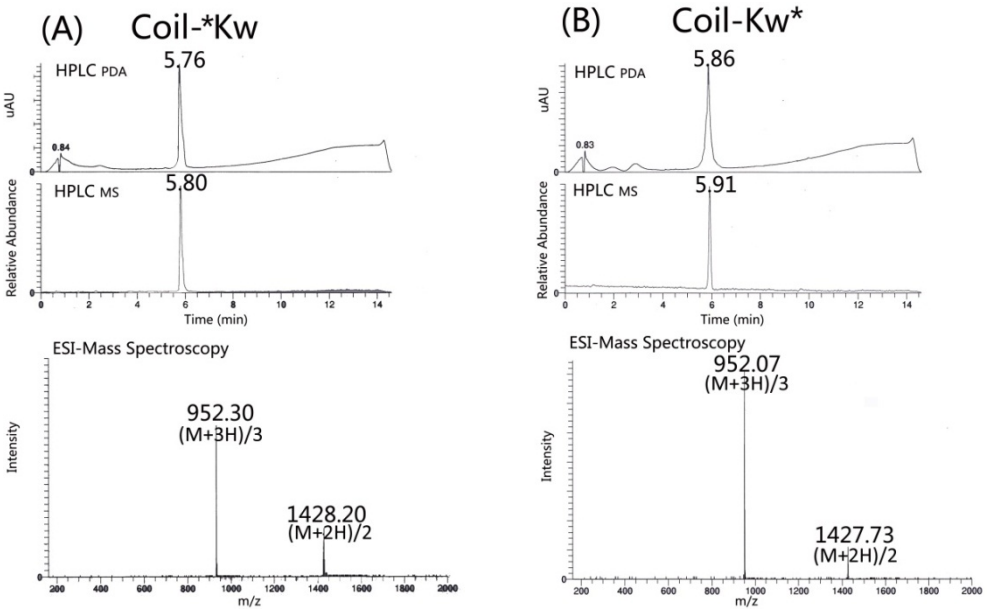

Figure A4. (A) LC-MS spectra of purified Coil-K_W^*, (B) LC-MS spectra of purified Coil-$^*K_W$. From top to bottom: UV (ultraviolet-visible) spectrum, ESI (electrospray ionization) spectrum, and mass spectrum.

Part 3. UV measurement for peptide concentration calculation

Lyophilized peptides may contain anywhere 10%~70% bound water and salts by weight. Therefore, it is better to ascertain the actual peptide concentration by UV spectroscopy.

The W and Y chromophore labeled peptide Coil-K and Coil-E concentration can be conveniently determined as follows:

1. Molar extinction coefficients (Ɛ) of chromophoric residues at neutral pH using a 1 cm cell:[65, 66]

Tryptophan (W) 5690 AU/mmole/ml, peak at 280.8 nm wavelength.

Tyrosine (Y) 1490 AU/mmole/ml, peak at 275.5 nm wavelength.

2. Calculations: peptide concentration (mol/L) $=(A_{peak} \times DF)/Ɛ$, where A_{peak} is the actual absorbance of the solution at peak value in a 1 cm cuvette, DF is dilution factor, MW is the molecular weight of the peptide and Ɛ is the molar extinction coefficient of each chromophore.

Part 4.CC-K/E CD thermal denaturation dissociation constant calculation

Summary of the original CC-K/E temperature denaturation parameters.

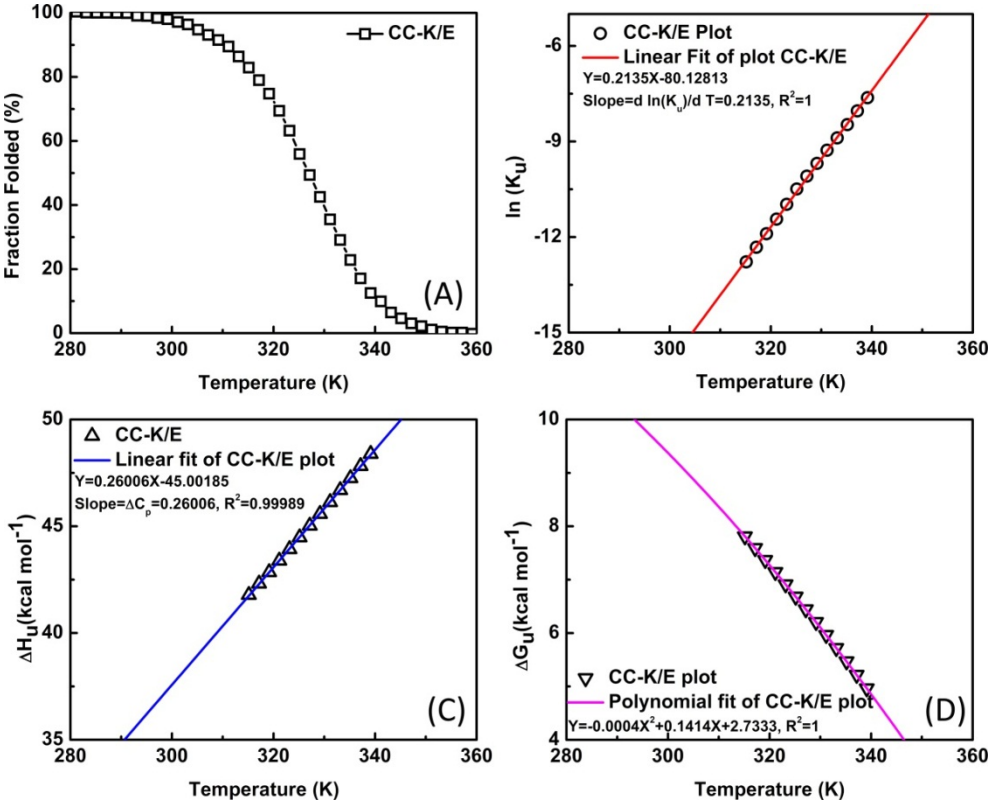

Figure A5. Thermal unfolding properties of CC-K/E. (A) Describes thermal dissociation curve of coiled coil complex CC-K/E, disassembling from 100% folding to 0% folding. Melting temperature is 331.15 K. (B) Describes the Van't Hoff plot of the thermal denaturation of CC-K/E. The dissociation constant at 25 ^{o}C is $K_u = 7.0 \times 10^{-8}$ M. (C) Describes the dependence of the enthalpy of unfolding of CC-K/E on temperature. (D) Describes free energy associated with the unfolding of CC-K/E as a function of temperature. The least-squares fit gives a ΔG^{H_2O} value at 25 ^{o}C of 9.33 kcal/mol. [Total peptide]= 40 μM, PBS pH 7.4.

Part 5. Hyperchem simulation of peptide structure[67]

Hyperchem release 8.0 package was used to simulate the peptide conformation and to determine the average distance between the spin label and the W (Tryptophan) aromatic amino acids in both peptide Coil-K_W^* and Coil-$^*K_W$.

For this, both Coil-K peptides were placed in a periodic box containing water molecules and the system was equilibrated at 300 K. The peptide can move in a constant-density environment which is similar to being in a liquid. The size of the box was set as a cube with W=H=D= 56.104 Å, and the minimum distance between solvent and solute atoms (atoms from peptides) is 2.3 Å.[88]

Molecular Mechanics simulation was based on a classical Newtonian calculation. Here, atoms were treated as Newtonian particles interacting through a potential energy function, which depend on bond lengths, bond angles, torsion angles, and non-bonded interactions (including van der Waals forces, electrostatic interactions, and hydrogen bonds). In these calculations, the forces on atoms are functions of the atomic position.

Furthermore, the AMBER force field which is typically used for developing proteins and nucleic acids was used to develop an all-atom model. The simulations were performed at 300 K with a 30 ps run time. Figures A6 shows the peptide comformation after simulation.

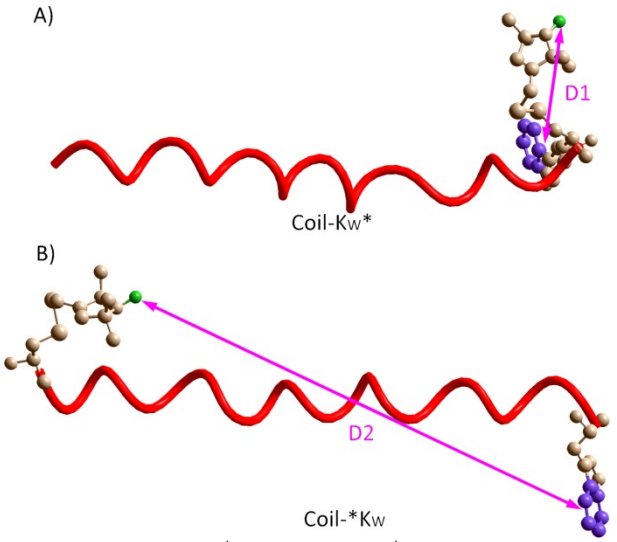

Figure A6. Structure of peptide Coil-K_W^* (A) and Coil-$^*K_W$ (B). In A) D1 indicates the distance between nitroxyl group and the W in peptide Coil-K_W^*. The average distance D1 is 6.6 Å. In B) the average distance D2 between the spin label and W is 36.7 Å.

Part 6. Molecular simulation

In the Martini model, groups of atoms (typically four) are united into specific interaction centers that absorb all the molecular detail of the replaced atoms. The coarse-grained particles interact via Lennard-Jones potential (with different well depth parameters depending on the specific pair type), screened electrostatic Coulomb potential, while the connectivity of the molecules is modeled by elastic bonds and angle potentials. By reducing the number of particles and the complexity of the interactions between them, longer simulation times can be achieved. Each of the five types of amino acids: E, A, I, L and K, constituting either Coil-K or Coil-E_r, is described at the coarse-grained level by an apolar interaction site representing the backbone and one or more interaction sites representing the side chains. The superposition of the atomistic and the coarse-grained representations of the CC-K/E coiled-coil structure is shown in Figure A7. The interaction parameters (hydrophobicity and polarity) for the coarse-grained particles have been set to closely reproduce the difference between particle's solvation free energy in polar and in apolar media. The α-helicity of the peptides is imposed through dihedral potentials along the backbone beads during the simulations.

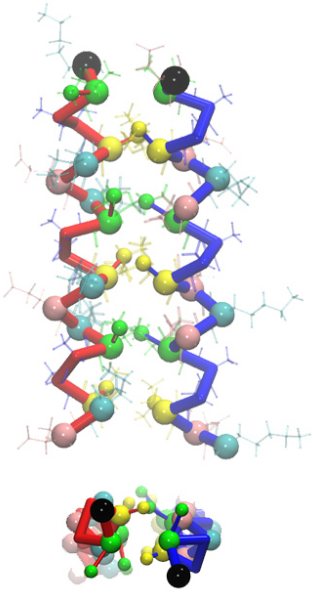

Figure A7. Lateral and top views of the parallel CC-K/E, as reported by Hodges group by NMR measurements. Red backbone stands for the secondary structure of peptide Coil-K; while blue backbone stands for the secondary structure of either peptide Coil-E. Green bead is Glutamic acid (E); cyan bead is Lysine (K); green bead is Isoleucine (I); yellow

bead is Leucine (K) amino acid. Alanine (A) amino acid is omitted here. For each peptide, the starting amino acid on N-terminus is colored in black. In the lateral view, the atomistic structure is overlaid, in transparent licorice representation.

In a typical simulation for this study, two Coil-K and two Coil-E_r peptides are randomly distributed (position and rotation randomness) in an 11 nm × 11 nm × 11 nm simulation box and solvated by water and ions, mimicking the buffer solution. At completion, the system consists of ~10000 coarse-grained particles: four peptides (21 amino acids for each), water particles (one coarse-grained water particle representing four real water moleules) and ions (Na^+ and Cl^-). Periodic boundary conditions in all directions were employed. Standard MARTINI simulations were used.[32] The Berendsen thermostat and barostat kept the temperature (t=300 K) and pressure (P=1 atm, isotropically) constant; the integration time step was t=20 fs.

Reference

1. A. Maximov, J. Tang, X. F. Yang, Z. P. P. Pang and T. C. Sudhof, *Science*, 2009, **323**, 516-521.
2. T. C. Sudhof and J. E. Rothman, *Science*, 2009, **323**, 474-477.
3. C. Hu, M. Ahmed, T. J. Melia, T. H. Sollner, T. Mayer and J. E. Rothman, *Science*, 2003, **300**, 1745-1749.
4. T. Weber, B. V. Zemelman, J. A. McNew, B. Westermann, M. Gmachl, F. Parlati, T. H. Sollner and J. E. Rothman, *Cell*, 1998, **92**, 759-772.
5. J. R. Litowski and R. S. Hodges, *Journal of Biological Chemistry*, 2002, **277**, 37272-37279.
6. H. Robson Marsden, A. V. Korobko, T. Zheng, J. Voskuhl and A. Kros, *Biomaterials Science*, 2013.
7. H. R. Marsden, N. A. Elbers, P. H. H. Bomans, N. Sommerdijk and A. Kros, *Angewandte Chemie-International Edition*, 2009, **48**, 2330-2333.
8. F. Versluis, J. Voskuhl, B. van Kolck, H. Zope, M. Bremmer, T. Albregtse and A. Kros, *Journal of the American Chemical Society*, 2013, **135**, 8057-8062.
9. T. Zheng, J. Voskuhl, F. Versluis, H. R. Zope, I. Tomatsu, H. R. Marsden and A. Kros, *Chemical Communications*, 2013, **49**, 3649-3651.
10. H. R. Marsden, I. Tomatsu and A. Kros, *Chemical Society Reviews*, 2011, **40**, 1572-1585.
11. T. T. Zheng, J. Voskuhl, F. Versluis, H. R. Zope, I. Tomatsu, H. R. Marsden and A. Kros, *Chemical Communications*, 2013, **49**, 3649-3651.
12. G. Pahler, C. Panse, U. Diederichsen and A. Janshoff, *Biophysical Journal*, 2012, **103**, 2295-2303.
13. F. Versluis, J. Dominguez, J. Voskuhl and A. Kros, *Faraday Discussions*, 2013.
14. P. R. E. Mittl, C. Deillon, D. Sargent, N. K. Liu, S. Klauser, R. M. Thomas, B. Gutte and M. G. Grutter, *Proceedings of the National Academy of Sciences of the United States of America*, 2000, **97**, 2562-2566.
15. M. E. Holtzer, E. Braswell, R. H. Angeletti, L. Mints, D. Zhu and A. Holtzer, *Biophysical Journal*, 2000, **78**, 2037-2048.
16. M. Goodman and M. Chorev, *Accounts of Chemical Research*, 1979, **12**, 1-7.
17. S. Lorenzen, C. Gille, R. Preissner and C. Frommel, *Febs Letters*, 2003, **545**, 105-109.
18. Y. Q. Deng, J. Liu, Q. Zheng, D. Eliezer, N. R. Kallenbach and M. Lu, *Structure*, 2006, **14**, 247-255.
19. S. R. Whitson, W. M. LeStourgeon and A. M. Krezel, *Journal of Molecular Biology*, 2005, **350**, 319-337.
20. A. Lombardi, C. M. Summa, S. Geremia, L. Randaccio, V. Pavone and W. F. DeGrado, *Proceedings of the National Academy of Sciences of the United States of America*, 2000, **97**, 6298-6305.
21. S. A. Palasek, Z. J. Cox and J. M. Collins, *Journal of Peptide Science*, 2007, **13**, 143-148.
22. H. Robson Marsden and A. Kros, *Angewandte Chemie (International ed. in English)*, 2010, **49**, 2988-3005.

23. T. Kaiser, G. J. Nicholson, H. J. Kohlbau and W. Voelter, *Tetrahedron Letters*, 1996, **37**, 1187-1190.
24. A. Y. Kornilova, J. F. Wishart, W. Z. Xiao, R. C. Lasey, A. Fedorova, Y. K. Shin and M. Y. Ogawa, *Journal of the American Chemical Society*, 2000, **122**, 7999-8006.
25. J. R. Litowski and R. S. Hodges, *Journal of Peptide Research*, 2001, **58**, 477-492.
26. S. M. Kelly and N. C. Price, *Biochimica Et Biophysica Acta-Protein Structure and Molecular Enzymology*, 1997, **1338**, 161-185.
27. S. M. Kelly, T. J. Jess and N. C. Price, *Biochimica Et Biophysica Acta-Proteins and Proteomics*, 2005, **1751**, 119-139.
28. P. Lavigne, M. P. Crump, S. M. Gagne, R. S. Hodges, C. M. Kay and B. D. Sykes, *Journal of Molecular Biology*, 1998, **281**, 165-181.
29. P. Lavigne, L. H. Kondejewski, M. E. Houston, F. D. Sonnichsen, B. Lix, B. D. Sykes, R. S. Hodges and C. M. Kay, *Journal of Molecular Biology*, 1995, **254**, 505-520.
30. A. L. Boyle, E. H. C. Bromley, G. J. Bartlett, R. B. Sessions, T. H. Sharp, C. L. Williams, P. M. G. Curmi, N. R. Forde, H. Linke and D. N. Woolfson, *Journal of the American Chemical Society*, 2012, **134**, 15457-15467.
31. B. Hess, C. Kutzner, D. van der Spoel and E. Lindahl, *Journal of Chemical Theory and Computation*, 2008, **4**, 435-447.
32. S. J. Marrink, H. J. Risselada, S. Yefimov, D. P. Tieleman and A. H. de Vries, *Journal of Physical Chemistry B*, 2007, **111**, 7812-7824.
33. L. Monticelli, S. K. Kandasamy, X. Periole, R. G. Larson, D. P. Tieleman and S. J. Marrink, *Journal of Chemical Theory and Computation*, 2008, **4**, 819-834.
34. D. Sengupta and S. J. Marrink, *Physical Chemistry Chemical Physics*, 2010, **12**, 12987-12996.
35. L. V. Schafer, D. H. de Jong, A. Holt, A. J. Rzepiela, A. H. de Vries, B. Poolman, J. A. Killian and S. J. Marrink, *Proceedings of the National Academy of Sciences of the United States of America*, 2011, **108**, 1343-1348.
36. X. Periole, A. M. Knepp, T. P. Sakmar, S. J. Marrink and T. Huber, *Journal of the American Chemical Society*, 2012, **134**, 10959-10965.
37. D. A. Lindhout, J. R. Litowski, P. Mercier, R. S. Hodges and B. D. Sykes, *Biopolymers*, 2004, **75**, 367-375.
38. S. A. Green, D. J. Simpson, G. Zhou, P. S. Ho and N. V. Blough, *Journal of the American Chemical Society*, 1990, **112**, 7337-7346.
39. N. V. Blough and D. J. Simpson, *Journal of the American Chemical Society*, 1988, **110**, 1915-1917.
40. P. L. Privalov, E. I. Tiktopulo and V. M. Tischenko, *Journal of Molecular Biology*, 1979, **127**, 203-216.
41. S. E. Herbelin and N. V. Blough, *Journal of Physical Chemistry B*, 1998, **102**, 8170-8176.
42. B. Pispisa, A. Palleschi, L. Stella, M. Venanzi and C. Toniolo, *Journal of Physical Chemistry B*, 1998, **102**, 7890-7898.
43. I. Solomon, *Physical Review*, 1955, **99**, 559-565.
44. N. Bloembergen and L. O. Morgan, *Journal of Chemical Physics*, 1961, **34**, 842-&.

45. J. Iwahara and G. M. Clore, *Nature*, 2006, **440**, 1227-1230.
46. C. Peggion, M. Jost, W. M. De Borggraeve, M. Crisma, F. Formaggio and C. Toniolo, *Chemistry & Biodiversity*, 2007, **4**, 1256-1268.
47. K. A. Bolin, P. Hanson, S. J. Wright and G. L. Millhauser, *Journal of Magnetic Resonance*, 1998, **131**, 248-253.
48. Z. O. Shenkarev, A. S. Paramonov, T. A. Balashova, Z. A. Yakimenko, M. B. Baru, L. G. Mustaeva, J. Raap, T. V. Ovchinnikova and A. S. Arseniev, *Biochemical and Biophysical Research Communications*, 2004, **325**, 1099-1105.
49. N. E. Zhou, C. M. Kay and R. S. Hodges, *Journal of Biological Chemistry*, 1992, **267**, 2664-2670.
50. S. Y. M. Lau, A. K. Taneja and R. S. Hodges, *Journal of Biological Chemistry*, 1984, **259**, 3253-3261.
51. B. Apostolovic and H. A. Klok, *Biomacromolecules*, 2008, **9**, 3173-3180.
52. Y. H. Chen, J. T. Yang and K. H. Chau, *Biochemistry*, 1974, **13**, 3350-3359.
53. N. J. Greenfield, *Nature Protocols*, 2006, **1**, 2733-2741.
54. R. Defrancesco, A. Pastore, G. Vecchio and R. Cortese, *Biochemistry*, 1991, **30**, 143-147.
55. J. M. Sturtevant, *Proceedings of the National Academy of Sciences of the United States of America*, 1977, **74**, 2236-2240.
56. T. Gruene, M. K. Cho, I. Karyagina, H. Y. Kim, C. Grosse, K. Giller, M. Zweckstetter and S. Becker, *Journal of Biomolecular Nmr*, 2011, **49**, 111-119.
57. J. Eisinger, B. Feuer and A. A. Lamola, *Biochemistry*, 1969, **8**, 3908-&.
58. F. Mito, T. Yamasaki, Y. Ito, M. Yamato, H. Mino, H. Sadasue, C. Shirahama, K. Sakai, H. Utsumi and K. Yamada, *Chemical Communications*, 2011, **47**, 5070-5072.
59. G. I. Likhtenstein, K. Ishii and S. Nakatsuji, *Photochemistry and Photobiology*, 2007, **83**, 871-881.
60. E. Gatto, G. Bocchinfuso, A. Palleschi, S. Oncea, M. De Zotti, F. Formaggio, C. Toniolo and M. Venanzi, *Chemistry & Biodiversity*, 2013, **10**, 887-903.
61. S. K. Chattopadhyay, P. K. Das and G. L. Hug, *Journal of the American Chemical Society*, 1983, **105**, 6205-6210.
62. C. V. Kumar, S. K. Chattopadhyay and P. K. Das, *Journal of the American Chemical Society*, 1983, **105**, 5143-5144.
63. W. A. Yee, V. A. Kuzmin, D. S. Kliger, G. S. Hammond and A. J. Twarowski, *Journal of the American Chemical Society*, 1979, **101**, 5104-5106.
64. F. Versluis, J. Dominguez, J. Voskuhl and A. Kros, *Faraday Discussions*, 2013.
65. H. Edelhoch, *Biochemistry*, 1967, **6**, 1948-&.
66. C. N. Pace, F. Vajdos, L. Fee, G. Grimsley and T. Gray, *Protein Science*, 1995, **4**, 2411-2423.
67. I. Hypercube, 2002, 2220.